Journal of Zhejiang University-SCIENCE A (Applied Physics & Engineering) 2025 26(6):499-511
www.jzus.zju.edu.cn; www.springer.com/journal/11582
E-mail: jzus_a@zju.edu.cn

Research Article

https://doi.org/10.1631/jzus.A2400045

Hydrodynamic characteristics of a wind turbine monopile foundation integrated with an oscillating water column wave energy device

Zhigang SHAN[1], Mengxia SONG[2], Jiapeng PAN[2], Baolong ZHANG[3], Miaojun SUN[1], Fang HE[2]✉

[1]*PowerChina HuaDong Engineering Co., Ltd., Hangzhou 311100, China*
[2]*Ocean College, Zhejiang University, Zhoushan 316021, China*
[3]*Zhejiang Provincial Energy Group Co., Ltd., Hangzhou 310007, China*

Abstract: We explore the incorporation of an oscillating water column (OWC) device into a monopile foundation designed for offshore wind power generation. The hydrodynamic characteristics of the structure are investigated, including the free water surface and air pressure response inside the OWC chamber, the wave energy capture performance, and the wave load response under various power take-off (PTO) damping and wave conditions. An orifice is employed to represent the quadratic PTO damping effect. Results indicate that increasing the PTO opening ratio increases the peak frequency of the water surface oscillation coefficient inside the OWC chamber, as well as the OWC pneumatic power. The load-reduction effect of the OWC device in the positive direction is likely related to the water surface oscillation inside the chamber and the wave energy extraction efficiency. At high wave frequencies, the water surface oscillation coefficient is relatively small, while the pneumatic power remains at a large value, and the OWC device can effectively reduce wave loads in the direction of incoming waves. The optimal opening ratio of 1.51% may balance wave energy utilization efficiency with structural protection for the device.

Key words: Oscillating water column (OWC); Offshore wind power; Monopile; Wave energy converter; Wave loads

1 Introduction

Global renewable energy production is expected to keep growing rapidly in the coming years. With its large-scale development and utilization, wind energy has gained maturity in the field of renewable energy (Liu et al., 2023). Offshore wind represents a new trend in wind power development, boasting favorable conditions such as high wind speed, small wind shear, low turbulence intensity, and long annual utilization hours (Liu et al., 2021). Monopile foundations, as a primary offshore wind power foundation type, display strong adaptability to water depth and mature construction technology, which can be applied even in deep-sea environments (Lee et al., 2023). However, the safety of monopile foundations in deep-sea conditions is of vital concern, due to the elevated wave loads they frequently encounter.

Many efforts have been made in the design of offshore wind power monopile foundations to reduce wave loads, such as using high-performance materials instead of steel pipes to reduce the monopile diameter (Ma and Yang, 2020), opening holes in the monopile hull to alter the flow patterns around the structure (Andersen et al., 2020), and attaching a shell to the foundation to reduce the flow resistance (Schopf, 2009). These measures can effectively decrease the area experiencing high forces or dissipate the wave energy, providing higher protection. In contrast to designs that dissipate wave power, a more favorable approach might involve the integration of wave energy converters (WECs) with wind power (Michele et al., 2019). This would enable the device to capture additional energy from waves, while effectively reducing the wave loads on the monopile foundations.

Wave energy is characterized by high predictability, utilization, and power density (He et al., 2023a). Many areas in the coastal waters of eastern China

✉ Fang HE, hefang@zju.edu.cn
Fang HE, https://orcid.org/0000-0002-5559-6230

Received Jan. 23, 2024; Revision accepted May 17, 2024;
Crosschecked Feb. 10, 2025; Online first Mar. 13, 2025

have been identified as suitable for wave energy development (Shi et al., 2022). WECs can be classified according to the types of power take-off (PTO) (Sheng, 2019). Among various WECs, the oscillating water column (OWC) device is the most widely used due to its simple structure and low number of mechanical components, displaying advantages of lower cost and higher durability (He et al., 2012; Falcão and Henriques, 2016; Zheng et al., 2020a). An OWC device consists of a fixed or floating pneumatic chamber with an underwater opening, in which water inside the chamber reciprocates to form an airflow. The airflow passes through a turbine fitted to the air chamber so that power can be generated.

Thus far, the main challenges to the widespread deployment of offshore OWC devices include high construction and maintenance costs (Chang et al., 2018). To improve cost-effectiveness, OWC devices have been integrated with breakwaters for additional benefits, including wave power supplementation and increased energy dissipation (He et al., 2016). The hydrodynamic characteristics of integration with various breakwater types, such as bottom landed (Boccotti et al., 2007; He and Huang, 2016; Kuo et al., 2017; Zheng et al., 2019, 2020b; Chen et al., 2020; Zhu et al., 2020; Zhao et al., 2022), pile supported (He and Huang, 2014; He et al., 2019; Qu et al., 2021), and floating (Koo, 2009; He et al., 2013, 2017; Howe et al., 2020; Ram et al., 2022), have been widely investigated.

More recently, OWC devices have been extended to offshore wind power monopile foundations, allowing efficient wave energy extraction along with foundation protection. The OWC device serves as an auxiliary module to provide power supplemental to the wind power. Besides utilizing a portion of wave energy, the process of vortex evolution in the flow field around the OWC device also dissipates a fair amount of wave energy (He et al., 2023b); thus, the wave loads on the monopile foundations can be significantly reduced. Moreover, due to the large-scale development of offshore wind power, the installation and maintenance costs of OWC devices can be considerably lowered.

A few previous studies have explored the integration of OWC devices into monopile foundations and investigated their hydrodynamic performance. For instance, Perez-Collazo et al. (2018) proposed a hybrid system consisting of an OWC device and a monopile foundation, and examined the hydrodynamic response of the OWC subsystem to different wave conditions. Similarly, Zhou et al. (2020) attached a shell-like OWC device to a monopile foundation, and evaluated the hydrodynamic performance and wave loads with numerical and experimental methods. Cong et al. (2021) proposed a four-chamber OWC device integrated into a monopile foundation, and numerically investigated its hydrodynamic performance using a higher-order boundary element method (HOBEM). It was found that the wave force on the four-chamber OWC device can be balanced by the wave force on the monopile foundation under certain conditions, resulting in essentially zero external force on the whole system. Li et al. (2022) also incorporated a cylindrical OWC device within a monopile foundation. The underwater opening of the OWC device was on the hull of the monopile foundation, with the hull of the monopile foundation forming the pneumatic chamber of the OWC device. As a result, no additional structural configuration was required. Compared to OWC devices integrated outside the monopile foundation, the proposed OWC device was more deeply integrated within the monopile foundation. Consequently, there was no increase in the amount of forced area, and improved wave load performance was expected. Up until now, the hydrodynamic performance of OWC monopiles has been investigated under different wave characteristics, chamber geometries, and PTO parameters. However, the effect of wave loads on OWC monopiles has not yet been studied.

In this study, the hydrodynamic performance of the OWC monopile proposed by Li et al. (2022) is experimentally investigated. Specifically, the air pressure fluctuation inside the chamber, water surface oscillation inside and outside the chamber, and wave energy extraction efficiency are analyzed. Moreover, the wave loads on the OWC monopile are examined and compared with an ordinary monopile of equal diameter. The practical load-reduction characteristics of the OWC monopile are verified for a sea state with wide wave frequencies, and an optimal PTO opening ratio is recommended. The results of this work can aid the design of multifunctional monopile foundations for offshore wind power, particularly in terms of wave energy extraction and foundation protections.

2 Experiments

2.1 Physical model and experimental setup

The experiments were carried out in a 25.00 m long, 0.70 m wide, and 0.70 m high wave flume in the Port Engineering Laboratory of the Ocean College, Zhejiang University, China. A piston-type wave maker equipped with an active wave-absorbing system is installed at one end of the flume, and a wave-absorbing beach with a 1∶6 slope covered with porous media is installed at the other end of the flume for reducing wave reflections. The pre-experimental results indicated that the wave-absorbing beach functioned effectively, with the wave reflections from the end being kept to less than 5% throughout the experiments.

Our model design followed the Froude similarity law. According to the dimensions of the wave flume and model prototype, a geometric scale factor of 1∶50 was adopted; thus, the time scale factor was 1∶7.07. Two sets of foundation models for offshore wind power were designed. The models were made of plexiglass. Model I was an OWC monopile, and Model II was an ordinary monopile with the same outer diameter as Model I. As Model II was a simple closed cylindrical structure, we do not present it here to save figure space. The geometric details of Model I are illustrated in Fig. 1. There is an arc-shaped opening of 0.10 m height and 120° on the side hull of the monopile. The opening is located underwater to communicate with the external fluid environment. From the bottom of the underwater opening and upwards, the monopile hull forms the pneumatic chamber of the OWC device. The outer diameter of the monopile D is 0.14 m, and the hull thickness δ is 0.005 m. Therefore, the diameter of the OWC chamber D_c is 0.13 m.

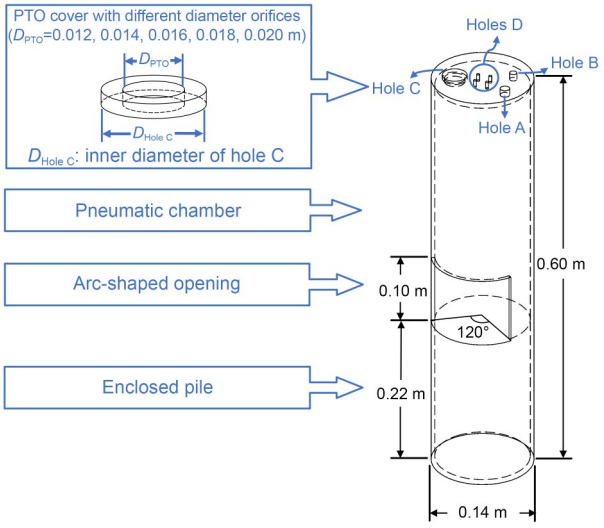

Fig. 1 Geometric details of Model I

In laboratory-scale tests, it is generally too difficult to fabricate a realistic mini-turbine, and instead, an orifice is commonly used to simulate an impulse turbine (He and Huang, 2017). This preserves the flow characteristics of a quadratic PTO mechanism. Different flow characteristics of the PTO mechanism can be simulated by replacing PTO covers with different orifice sizes. The influence of PTO damping on Model I was the focus of this study, and five orifice diameters (D_{PTO}=0.012, 0.014, 0.016, 0.018, and 0.020 m) were tested. The corresponding opening ratios (e), i.e., the area of the aperture opening divided by the cross-sectional area of the OWC chamber, were 0.85%, 1.16%, 1.51%, 1.92%, and 2.37%, respectively, covering a broad range. As shown in Fig. 1, several holes (A–D) existed on the top of Model I for installing sensors and PTO cover. After installation, the connections between the holes and sensors were all sealed. As a result, the air above the water column inside the OWC chamber could only pass through the orifices in the PTO cover. Incidentally, the study by Hayati et al. (2020) indicates that altering the position of the PTO cover of the OWC device does not significantly affect the wave energy conversion efficiency. Therefore, the position of the PTO cover in Model I was not strictly controlled. From the perspective of wave energy utilization rate in engineering applications, the energy-capturing effect of the PTO cover at any position on the top of the OWC chamber (or even on the side hull of the OWC chamber) is similar, and the PTO cover installation location can be optimized based on field conditions.

As illustrated in Fig. 2, Model I was positioned at a distance of 13 m away from the wave maker in the experiments. The force chain was used to measure the wave loads on the model. The model was firmly mounted to the force chain, with a 0.02 m gap between the monopile bottom and the flume bottom. Consequently, there was no bottom friction affecting the total horizontal wave force measurement, and the gap was small and deep enough to avoid large vertical wave force on the monopile bottom. Three wave gauges (WG1–WG3) were used to measure the instantaneous surface elevation. WG1 was 5.00 m away

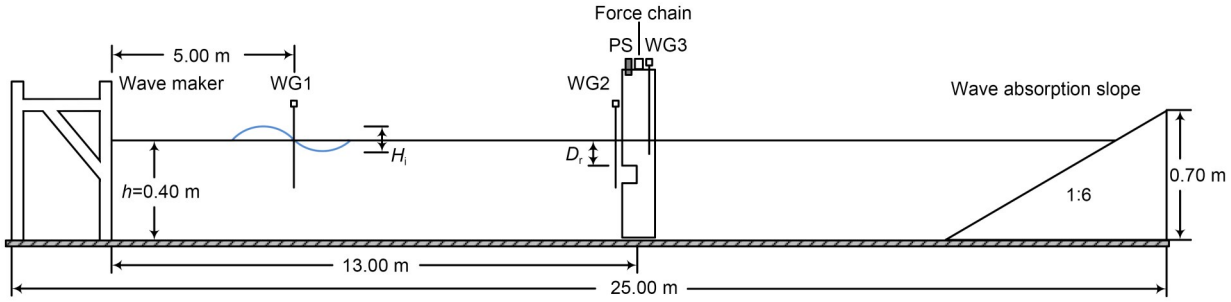

Fig. 2 Schematic diagram of the experimental setup

from the wave maker to measure the incident wave height, WG2 was 0.04 m in front of the model's wave-facing surface to measure the water surface oscillation outside the OWC chamber, and WG3 was on the model to measure the water surface oscillation inside the OWC chamber. The air pressure sensor (PS) was used to measure the air pressure fluctuation inside the OWC chamber. Since Model II does not have an air chamber, WG3 and PS were not installed. Apart from this, the installation location of Model II and the mounting positions of the remaining sensors were the same as those depicted in Fig. 2.

The wave gauges and force chain were recalibrated before and after the experiments on each day to ensure measurement accuracy. The sampling frequency was 100 Hz for all sensors. All sensors were connected to a synchronous collector to ensure that all data were recorded in the same time series.

2.2 Testing conditions

In this study, the water depth h was kept at 0.40 m for all test conditions, and so the draft of the OWC chamber D_r was fixed at 0.06 m. The wave period T was varied from 0.70 s to 1.60 s at an interval of 0.10 s, and the target incident wave height H_i was varied from 0.03 m to 0.06 m at an interval of 0.01 m. The arc-shaped opening on the side hull of the monopile was kept underwater throughout all experiments to avoid air leakage. We used the dimensionless wave number kh to present the results, where k denotes the wave number. For the range of the tested wave period, kh varied from 0.89 to 3.30. Details of the testing conditions are summarized in Table 1 for reference.

2.3 Analysis methods

According to the linear wave theory, the incident energy flux P_I per unit of wave-crest length can be expressed as:

Table 1 Summary of test conditions

Parameter	Value
Water depth, h	0.40 m
Incident wave height, H_i	0.03–0.06 m (with an interval of 0.01 m)
Wave period, T	0.70–1.60 s (with an interval of 0.10 s)
Wave angle, β	0°

$$P_I = \frac{1}{16}\frac{\rho g H_i^2 \sigma}{k}\left[\frac{2kh}{\sinh(2kh)}+1\right], \tag{1}$$

where ρ is the water density; g is the gravitational acceleration; σ is the wave angular frequency, $\sigma = \frac{2\pi}{T}$, satisfying the dispersion equation as:

$$\sigma^2 = gk\tanh kh, \tag{2}$$

where the wave number k can be determined for a given wave angular frequency σ and water depth h. The pneumatic power P_E extracted by the OWC chamber from the wave field within one wave period can be calculated by:

$$P_E = \frac{S}{T}\int_{t_0}^{t_0+T} p(t)u(t)\mathrm{d}t, \tag{3}$$

where S is the cross-sectional area of the OWC chamber; t_0 is a selected starting moment after the experimental test has reached the steady state; $p(t)$ is the measured air pressure inside the OWC chamber; $u(t)$ is the vertical velocity of the water surface inside the chamber; t is the time.

In the experiments, the capture width ratio C_c is used to quantify the wave energy extraction capacity of the OWC device, which is defined as:

$$C_c = \frac{P_E}{P_I D_c}. \tag{4}$$

The pressure coefficient C_p representing the air pressure fluctuation inside the OWC chamber is defined as (He and Huang, 2016):

$$C_p = \frac{\Delta p}{\rho g H_i}, \tag{5}$$

where Δp is the difference between the maximum and minimum values of $p(t)$ inside the chamber. The amplifying coefficient C_a representing the water surface oscillation inside the OWC chamber is defined as:

$$C_a = \frac{\Delta \eta}{H_i}, \tag{6}$$

where $\Delta \eta$ is the difference between the maximum and minimum values of $\eta(t)$, which is the water surface elevation inside the OWC chamber as measured by the wave gauge WG3. The ratio of load reduction R_L is used to characterize the effect of the OWC device in reducing wave loads on the monopile, and is given by:

$$R_L = \frac{F_{max}^{II} - F_{max}^{I}}{F_{max}^{II}} \times 100\%, \tag{7}$$

where F_{max}^{II} is the maximum horizontal wave load of Model II; F_{max}^{I} is the maximum horizontal wave load of Model I. A positive R_L value means that the OWC device exerts a load-reduction effect.

3 Results

3.1 Water surface oscillation

The relationship between the in-chamber water surface oscillation coefficient C_a and the dimensionless wave number kh is shown in Fig. 3, for different incident wave heights H_i under five different PTO conditions. It should be noted that increasing H_i will correspondingly decrease C_a, except for some specified experimental cases with large opening ratios e and low wave frequencies. This may be explained by the quadratic damping effect of the orifice. The larger the incident wave height H_i, the stronger the free water surface oscillation inside the chamber, which results in a larger air pressure inside the OWC chamber. Because of the quadratic damping effect of the orifice, the air pressure inside the chamber increases more and more quickly with the increase of the air volume flow rate, leading to a decrease in C_a. When the chamber is

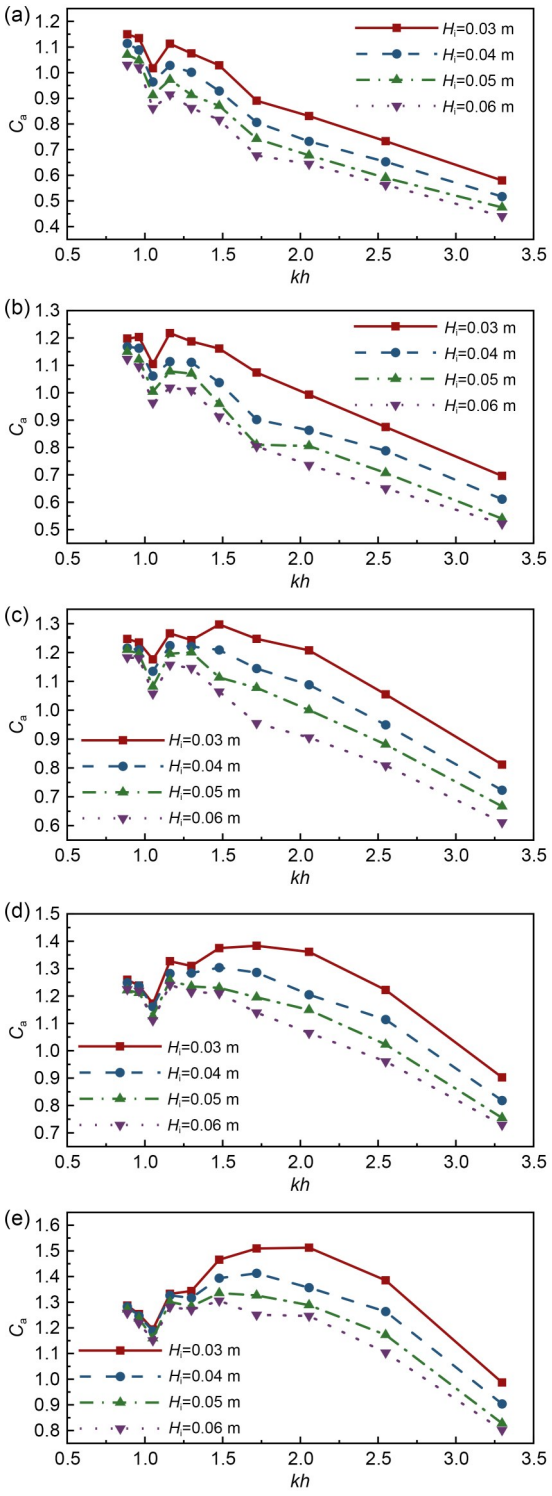

Fig. 3 Variation of in-chamber water surface oscillation coefficient C_a versus kh for different values of H_i with: (a) e=0.85%; (b) e=1.16%; (c) e=1.51%; (d) e=1.92%; (e) e=2.37%

equipped with an orifice whose opening ratio e is large enough, the PTO damping effect could be equivalent to linear damping for low-frequency wave conditions, where C_a is nearly independent of the changes in H_i.

It is worth noting that the curves of C_a exhibit a local minimum around kh=1.05 (Fig. 3), which appears to be insensitive to the change of the incident wave height H_i and the opening ratio e. However, neither significant natural vibration of the model nor an unusual inhomogeneity of the water surface inside the chamber were observed in the experiments around kh=1.05. We believe that the appearance of the local fluctuation in the trend of the C_a curves may be related to the flow characteristics at the side hull opening of the device, although this hypothesis needs to be verified by further investigation of the flow field around the OWC monopile.

In addition to the local minimum mentioned above, there are other noteworthy peaks. As the opening ratio e increases, a set of peaks appears on the curves of C_a and then shifts toward higher wave frequencies (Fig. 3). The case at H_i=0.03 m is a typical example. When e=0.85%, the curve of C_a basically follows a decreasing trend with kh (Fig. 3a). A peak begins to appear when e=1.16%, with a frequency of kh=1.16 (Fig. 3b). Subsequently, when e gradually increases to 2.37%, the peak shifts to a higher frequency of kh=2.06 (Figs. 3c–3e). This phenomenon is observed at each test group for different incident wave heights, but is less pronounced when the incident wave height is relatively large. For example, for the relatively large incident wave height of H_i=0.06 m, the peak does not start to appear until the opening ratio e=1.92% (Fig. 3d), and there is a slight frequency shift when the opening ratio continues to increase to e=2.37% (Fig. 3e).

This phenomenon can be explained as follows. When the air volume flow rate is small or the orifice opening size is large enough, the nonlinear effect of the orifice damping may not be fully reflected, and the orifice effect is essentially equivalent to linear damping, i.e., the damping coefficient is approximately a constant value and independent of the air volume flow rate. When the air volume flow rate is large or the orifice opening size is small, the quadratic damping effect of the orifice becomes quite strong, and a small change in the volume flow rate could lead to a much larger change in the air pressure inside the chamber, compared to when the air volume flow rate is small. For such circumstances, the strong nonlinearity of the orifice is not like linear damping, and a non-negligible increase of the instantaneous damping coefficient occurs with the increase of air volume flow rate. Under this damping effect, the increase of kh causes the water surface oscillation inside the chamber to accelerate, and the air volume flow rate increases, increasing the damping sharply. The air pressure inside the chamber then increases too quickly, inhibiting the water surface oscillation.

For large opening ratios, the quadratic effect of the orifice damping is more difficult to fully reflect. Therefore, at low wave frequencies, the air volume flow rate is small and the damping coefficient is approximately a low constant value. As kh increases, the velocity and acceleration of water particles near the wave surface are greater, and the water exchange through the side hull opening of the OWC monopile becomes more pronounced. At this time, C_a increases with kh. However, if kh continues to increase, the air volume flow rate becomes larger, causing the orifice to again show a quadratic damping effect. The air pressure inside the chamber then increases with large damping, and the inhibition of the water surface oscillation inside the chamber gradually increases. As a result, the C_a curve will reach a peak and then decrease. The change in damping effects also explains why the peak shifts to higher wave frequencies with increasing opening ratios. This is because for orifices with larger opening ratios, a larger air volume flow rate (i.e., a larger kh) is required for the orifice to exhibit quadratic damping. In addition, the water surface oscillation inside the chamber would cause a greater air volume flow rate with greater H_i. In this case, the increase of kh is more likely to cause a non-negligible increase of the instantaneous damping coefficient, which makes the shift in peak frequency more subtle.

3.2 Air pressure fluctuation

Fig. 4 presents the data associated with the opening ratio e=1.51%, in which the curves show the variation of air pressure coefficient C_p versus the dimensionless wave number kh for different incident wave heights H_i. The curve shapes and peak frequencies of C_p corresponding to the remaining opening ratios are similar (Fig. S1 of the electronic supplementary material). C_p is positively correlated with H_i, and the C_p curve shifts upwards as H_i increases. This is mainly

because when H_i becomes larger, the free water surface fluctuation inside the chamber is enhanced, and the air volume flow rate increases. The existence of the quadratic damping effect of the orifice makes the air pressure fluctuation above the water surface larger, resulting in an increase in C_p inside the chamber.

C_p increases as kh increases, reaching a maximum value at a certain wave frequency representing (or close to) the chamber resonant frequency (Elhanafi and Kim, 2018), and then decreases with a further increase in kh. The peak frequency of C_p is at kh=2.55 for H_i=0.03 m and at kh=2.06 for all other incident wave height test groups; thus, it can be inferred that the chamber resonant frequency should be within kh=2.00–2.50. Near the peak frequency and at higher frequencies, the change in the amplitude of air pressure fluctuation inside the chamber resulting from changes in incident wave height is not significant. However, it becomes more pronounced in lower-frequency waves, far from the peak frequency. For example, as shown in Fig. 4, when H_i changes from 0.03 m to 0.06 m, C_p only increases by 10% when kh=2.06, yet C_p increases by 78% when kh=0.89.

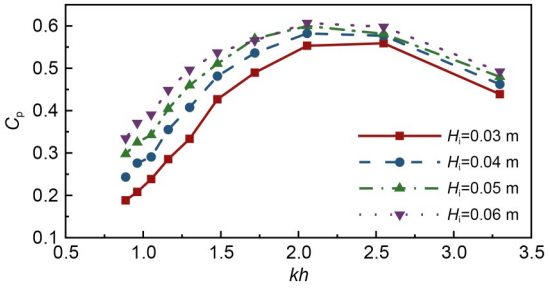

Fig. 4 Variation of the air pressure coefficient C_p versus kh for different values of H_i with e=1.51%

3.3 Wave energy extraction capacity

The variation curves of pneumatic power P_E versus the dimensionless wave number kh under five different PTO conditions, when H_i=0.04 m, are shown in Fig. 5a. With the increase of kh, P_E first increases and then gradually decreases after reaching a peak. Although the change of PTO has no significant effect on the overall trend, the peak frequency of P_E continues to shift to higher frequency with increasing e. For instance, the peak frequency of P_E when e=0.85% occurs at kh=1.48, while for e=2.37% it is observed at kh=2.06. This is similar to the effect of changing e in Fig. 3. As mentioned in Section 3.1, the change of e directly affects the response of the free water surface and air pressure in the OWC chamber. For the OWC monopile, the free water surface oscillation fluctuation inside the chamber causes air pressure oscillation above, as well as air flow rate changes at the orifice. A similar trend of an increase in peak frequency with the increase of the opening ratio is observed in the P_E curves, mirroring the behavior seen in the C_a curves. As shown in Fig. 5a, when kh is higher than 1.50, the opening ratio e=1.51% results in more extracted wave energy than the other examined opening ratios. Accordingly, P_E is about 1.05–1.16 times of that for e=0.85%, and the peak frequency of P_E appears at kh=2.06. When kh is lower than 1.50 in the examined cases, P_E decreases with the increase of e.

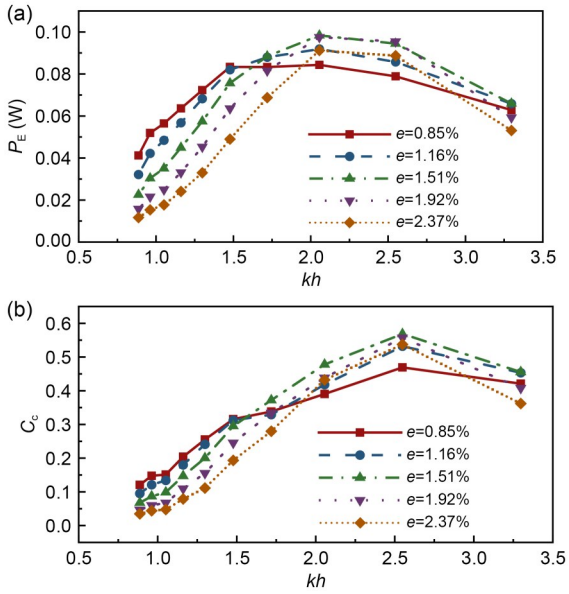

Fig. 5 Variation of (a) the pneumatic power P_E and (b) the capture width ratio C_c versus kh for different values of e with H_i=0.04 m

The variation curves of capture width ratio C_c versus the dimensionless wave number kh under five different PTO conditions, for H_i=0.04 m, are illustrated in Fig. 5b. Similar to the trend of the P_E curves, as kh increases, C_c first increases to a peak and then gradually decreases. However, the peak frequency of C_c is insensitive to the change of e, and the peak frequency under each opening ratio consistently occurs at kh=2.51. One can conclude that if the main wave frequency range of the particular sea state is wide and relatively large (kh>1.5), e=1.51% could be the optimal opening ratio of the OWC device. With this configuration, the

OWC device's output power could be maintained at a relatively high level.

Incident wave height has an important impact on the capture value and extraction efficiency of wave energy. Taking the experiments with an opening ratio of e=1.51% as an example, Fig. 6 shows the effects of the incident wave height H_i on the frequency responses of the pneumatic power P_E and the capture width ratio C_c. As expected, P_E increases significantly with the increase of H_i, indicating that the OWC device can extract more wave energy in a sea state with larger wave heights. According to Fig. 6a, when H_i changes from 0.03 m to 0.06 m, i.e., the incident wave height doubles, P_E increases by a factor of 3.38–6.87. This phenomenon is similar to the remaining opening ratio conditions (Fig. S2 of the electronic supplementary material).

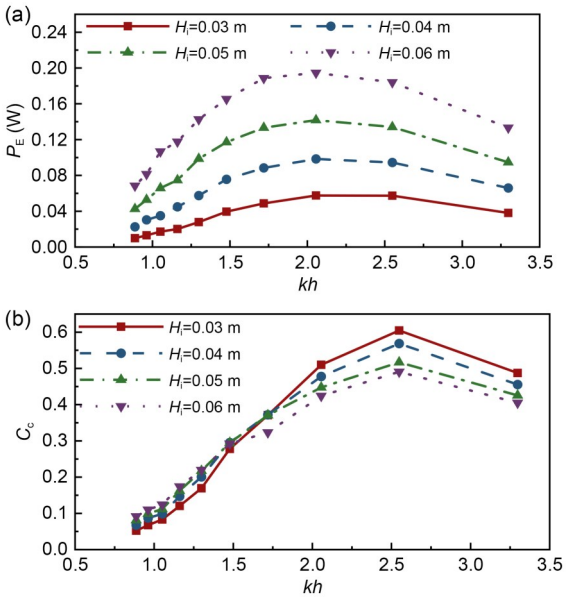

Fig. 6 Variation of (a) the pneumatic power P_E and (b) the capture width ratio C_c versus kh for different values of H_i with e=1.51%

The trend of C_c with H_i at different wave frequencies is not consistent. As shown in Fig. 6b, when kh is less than 1.50, C_c increases with the increase of H_i. In contrast, the opposite trend is observed when kh is greater than 1.50. One possible reason for this is that since the wavelengths are short, the increase of H_i will intensify the free water surface oscillation in the OWC chamber, and make the spatial distribution of the free water surface inside the chamber more uneven, resulting in greater energy dissipation (Li et al., 2022). Overall, the peak of C_c occurs at H_i=0.03 m and kh=2.55.

3.4 Wave loads

We next compared the wave loads of the OWC monopile with those of a traditional offshore wind power monopile, to verify the safety and engineering feasibility of the new integrated structure. The water depth and the incident wave height are kept at h= 0.40 m and H_i=0.04 m, respectively, for the wave load measurement. The ratios of load reduction R_L in the direction of incoming waves (defined as the positive direction) and the opposite direction of incoming waves (defined as the negative direction) are shown in Figs. 7a and 7b, respectively, as a function of the dimensionless wave number kh under different opening ratios.

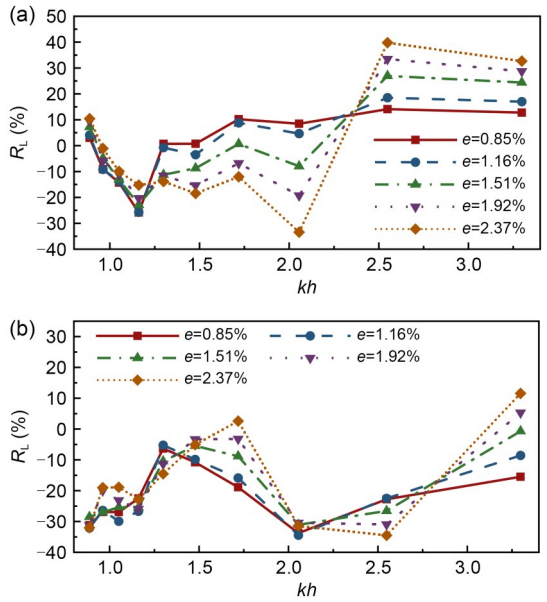

Fig. 7 Variation of the ratio of load reduction R_L versus kh for different values of e with H_i=0.04 m in (a) the positive direction and (b) the negative direction

As seen in Fig. 7a, we divide the results into three wave frequency ranges based on the load-reduction effect of the OWC monopile on wave loads in the positive direction. At high wave frequencies (kh≥2.50), the OWC device shows a load-reduction effect, which is more obvious as e increases. At medium wave frequencies (kh=1.30–2.50), the load-reduction effect of the OWC device is highly correlated with the opening ratio. For small opening ratios (i.e., e=0.85% and e= 1.16%), the OWC device can reduce loads, or at least

maintain zero or slight increases in loads. However, as the opening ratio increases, the OWC monopile will be subjected to an additional wave load burden. At low wave frequencies (kh≤1.30), the load characteristics of the OWC monopile are mainly affected by kh rather than the opening ratio. With the increase of kh, the effect of the OWC device gradually shifts from load reduction (R_L>0) to load increase (R_L<0).

The variation of R_L in the positive direction may be explained by the trend of the in-chamber water surface oscillation coefficient C_a and pneumatic power P_E (Figs. 3 and 5). A larger oscillation of the in-chamber water surface indicates better water exchange through the side hull opening, as well as more prominent momentum transfer between the water particles and the structure. As a result, a relatively large value of C_a typically corresponds to a large wave load in the positive direction on the OWC monopile. In addition, since the OWC device only extracts a portion of the incident wave energy, an increase in P_E can theoretically reduce wave loads on the OWC monopile. At low wave frequencies, C_a is kept at a large value for different opening ratios; meanwhile, the value of P_E is small. As a result, the monopile's wave load is increased after the integration of the OWC device. The value of P_E stays high for medium wave frequencies, although it does fluctuate when the opening ratio changes. However, C_a changes significantly depending on the opening ratios. At medium wave frequencies, the value of C_a is smaller for small opening ratios and larger for large opening ratios, compared to low wave frequencies. As the opening ratio increases, the peak of the C_a curve with H_i=0.04 m appears, and the peak frequency shifts from low to medium wave frequencies. As a result, in medium-frequency waves, the OWC device at large opening ratios increases the wave loads on the monopile, while at small opening ratios (i.e., e=0.85% and e=1.16%), the loads can even reduce (Fig. 7a). At high wave frequencies, C_a is kept low, while the value of P_E is high. Therefore, the OWC device displays a strong load-reduction effect at high wave frequencies.

The load characteristics of the OWC monopile in the negative direction are shown in Fig. 7b. In most cases, the OWC device applies an additional wave load burden on the monopile, especially at low wave frequencies (kh≤1.30) and medium-high wave frequencies (kh=2.06–2.55), where the absolute increment of R_L can be up to 20%–40%. A set of peaks appears on the R_L curves with kh=1.30–1.72, where wave loads in the negative direction on the OWC device do not increase much at all, or even reduce slightly (kh=1.72 and e=2.37%). From the results of water surface oscillation, air pressure fluctuation, and wave energy extraction capacity, it is challenging to summarize a definitive explanation for the fluctuations of the R_L curves in the negative direction. For the negative direction flow in the oscillatory flow field, the geometrical boundaries of the side hull opening may produce complex vortex shedding, which could be the reason for large wave loads upon the OWC monopile.

It is worth noting that in Fig. 7, at a particularly high wave frequency of kh=3.30, wave loads in the positive direction are significantly reduced, and meanwhile wave loads in the negative direction are not overburdened. This is in keeping with our results, since we found that for a certain incident wave height, water depth, and pile diameter, the wave load for the monopile in the positive direction from high-frequency waves tends to be the maximum horizontal wave load (F_{Hmax}) in a wide-frequency sea state (i.e., a realistic sea state encompassing many frequencies of waves) (Fig. 8). Considering wide wave frequencies, the OWC device reduces the maximum horizontal wave load in the positive direction, except for when the opening ratio is large (i.e., e=2.37%), which causes a load surge at kh=2.06 (Fig. 8a). The maximum horizontal wave load in the negative direction increases for the OWC monopile compared to a traditional monopile. However, it does not exceed the maximum horizontal wave load in the positive direction (Fig. 8b). Overall, while OWC devices with large opening ratios show better load-reduction effects in both directions at high wave frequencies, they perform poorly for load reduction in the positive direction at medium wave frequencies. Therefore, it is recommended to use medium opening ratios (e.g., e=1.16% or e=1.51%) to obtain a better load-reduction effect.

The OWC monopile exhibits good load-reduction characteristics upon experiencing very high frequency waves. Thus, we further explore the effects of different incident wave heights H_i and opening ratios e on the ratio of load reduction R_L when kh=3.30. According to Fig. 9, the load-reduction performance of the OWC monopile deteriorates as H_i increases. As H_i increases, the incident wave energy flux also increases. We discussed earlier that the increase of H_i

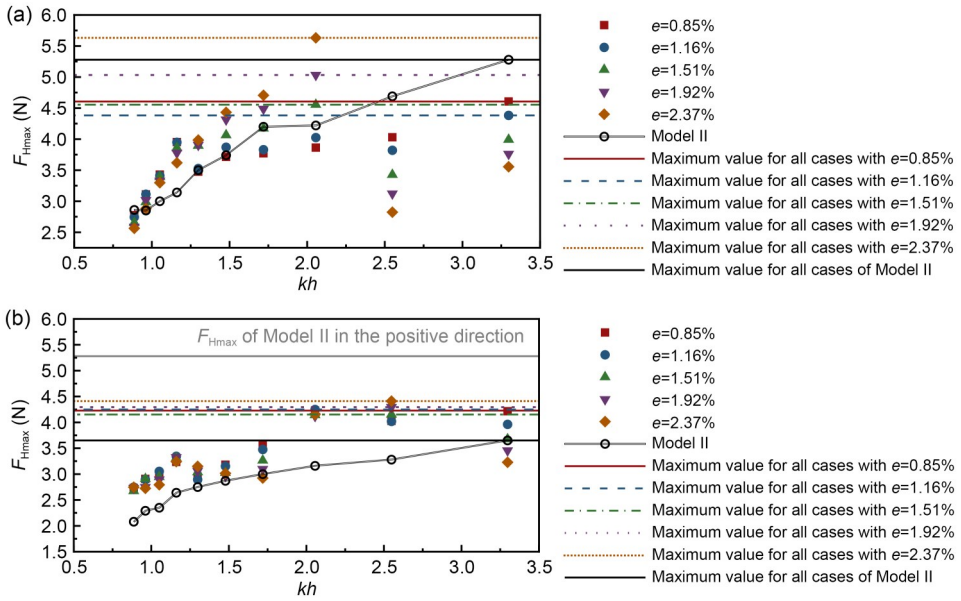

Fig. 8 Variation of the maximum horizontal wave load for Models I and II under five different PTO conditions in (a) the positive direction and (b) the negative direction

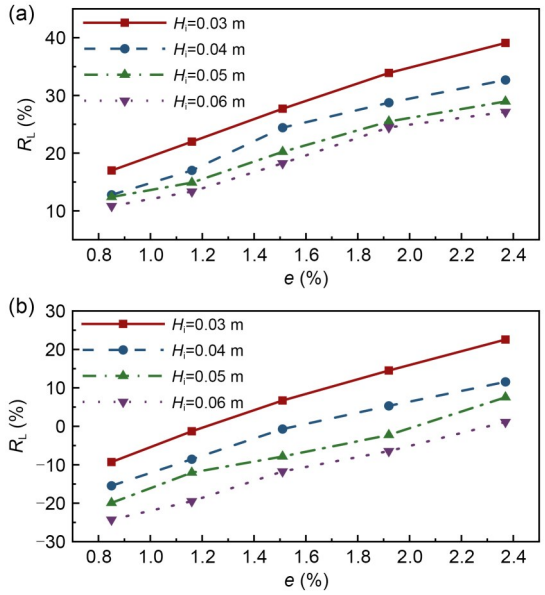

Fig. 9 Variation of the ratio of load reduction R_L versus e for different values of H_i with kh=3.30 in (a) the positive direction and (b) the negative direction

can effectively increase the pneumatic power P_E so that more wave energy is extracted per unit time, but this effect is clearly not enough to fully compensate for the increase in wave energy flux. Therefore, wave loads on the OWC monopile increase, and the value of R_L correspondingly decreases.

For offshore wind farms that experience high frequency waves for long durations, the load reduction offered by the OWC monopile will be particularly useful. Furthermore, compared with traditional monopiles, the OWC monopiles have the unique advantage of complementary wind-wave energy utilization, making their improved energy efficiency an important consideration in addition to their structural protection benefits. Considering the energization characteristics of the OWC device in Fig. 5, and the load-reduction characteristics in Figs. 7 and 8, we recommend choosing a medium opening ratio (e.g., e=1.51%). With a medium opening ratio, the OWC device maintains high wave energy utilization efficiency and good load-reduction ability in a wide-frequency sea state.

4 Conclusions

We experimentally investigated the hydrodynamic characteristics, wave energy utilization efficiency, and wave load characteristics of an offshore monopile foundation integrated with an OWC device (OWC monopile).

The in-chamber water surface oscillation coefficient C_a and the pneumatic power P_E were found to be affected by the height and frequency of incident waves. Specifically, all results showed that with the increase of the opening ratio e, the peak frequencies of the C_a and P_E curves shift to higher wave frequencies.

This is mainly due to the orifice-induced quadratic damping, which presents different equivalent linear damping effects depending on the air volume flow rate.

Additionally, the wave load characteristics in the positive direction of the OWC monopile are related to the water surface oscillations inside the chamber, as well as the wave energy extraction power of the OWC device. In particular, an OWC device with a smaller C_a and a larger P_E shows a better load-reduction effect in the positive direction.

The OWC device can reduce the positive wave loads in high wave frequencies, thus reducing the maximum horizontal wave load on the monopile in wide-frequency sea states for most cases. However, a large opening ratio is not suitable because it will lead to a load surge at medium wave frequencies. Therefore, in order to achieve a better load-reduction effect, medium opening ratios should be used (e.g., e=1.16% or e=1.51%).

An opening ratio of approximately e=1.51% should be used to fully leverage the advantages of the OWC-integrated structure, in terms of both the wave energy utilization efficiency and the load-reduction effect. This opening ratio not only displays its advantages at high wave frequencies (i.e., achieving the highest wave energy capture efficiency and good load-reduction effect), but also demonstrates strong adaptability to low- and medium-frequency sea states.

It is worth noting that this study focused on hydrodynamic behavior, and a detailed structural engineering analysis of OWC monopiles. For instance, using the finite element method should be performed to ensure that the structural strength meets the criteria during the design phase. Also, further study of the flow field details would be beneficial for understanding wave energy dissipation. In addition, in this work, we only considered normal incident waves. The load characteristics of the OWC monopile for different incident wave angles may be an interesting avenue for further study.

Acknowledgments

This work is supported by the "Pioneer" R&D Program of Zhejiang (No. 2022C03009), the National Natural Science Foundation of China (Nos. 52022092, 51979247, and 52211530092), the Talent Program of Zhejiang Province (No. 2021R52050), and the Natural Science Foundation of Zhejiang Province (No. LZ23E090001), China.

Author contributions

Zhigang SHAN: conceptualization, methodology, writing–review & editing, resources, and supervision. Mengxia SONG: formal analysis, investigation, writing–original draft, and data curation. Jiapeng PAN: investigation, writing–original draft, and visualization. Baolong ZHANG: investigation and writing–original draft. Miaojun SUN: investigation and writing–review & editing. Fang HE: conceptualization, methodology, writing–review & editing, supervision, and funding acquisition.

Conflict of interest

Zhigang SHAN, Mengxia SONG, Jiapeng PAN, Baolong ZHANG, Miaojun SUN, and Fang HE declare that they have no conflict of interest.

References

Andersen J, Abrahamsen R, Andersen TL, et al., 2020. Wave load mitigation by perforation of monopiles. *Journal of Marine Science and Engineering*, 8(5):352. https://doi.org/10.3390/jmse8050352

Boccotti P, Filianoti P, Fiamma V, et al., 2007. Caisson breakwaters embodying an OWC with a small opening—part II: a small-scale field experiment. *Ocean Engineering*, 34(5-6):820-841. https://doi.org/10.1016/j.oceaneng.2006.04.016

Chang G, Jones CA, Roberts JD, et al., 2018. A comprehensive evaluation of factors affecting the levelized cost of wave energy conversion projects. *Renewable Energy*, 127:344-354. https://doi.org/10.1016/j.renene.2018.04.071

Chen J, Wen HJ, Wang YX, et al., 2020. Experimental investigation of an annular sector OWC device incorporated into a dual cylindrical caisson breakwater. *Energy*, 211:118681. https://doi.org/10.1016/j.energy.2020.118681

Cong PW, Teng B, Bai W, et al., 2021. Wave power absorption by an oscillating water column (OWC) device of annular cross-section in a combined wind-wave energy system. *Applied Ocean Research*, 107:102499. https://doi.org/10.1016/j.apor.2020.102499

Elhanafi A, Kim CJ, 2018. Experimental and numerical investigation on wave height and power take-off damping effects on the hydrodynamic performance of an offshore–stationary OWC wave energy converter. *Renewable Energy*, 125:518-528. https://doi.org/10.1016/j.renene.2018.02.131

Falcão AFO, Henriques JCC, 2016. Oscillating-water-column wave energy converters and air turbines: a review. *Renewable Energy*, 85:1391-1424. https://doi.org/ 10.1016/j.renene.2015.07.086

Hayati M, Nikseresht AH, Haghighi AT, 2020. Sequential optimization of the geometrical parameters of an OWC device based on the specific wave characteristics. *Renewable Energy*, 161:386-394. https://doi.org/10.1016/j.renene.2020.07.073

He F, Huang ZH, 2014. Hydrodynamic performance of

pile-supported OWC-type structures as breakwaters: an experimental study. *Ocean Engineering*, 88:618-626. https://doi.org/10.1016/j.oceaneng.2014.04.023

He F, Huang ZH, 2016. Using an oscillating water column structure to reduce wave reflection from a vertical wall. *Journal of Waterway, Port, Coastal, and Ocean Engineering*, 142(2):04015021. https://doi.org/10.1061/(ASCE)WW.1943-5460.0000320

He F, Huang ZH, 2017. Characteristics of orifices for modeling nonlinear power take-off in wave-flume tests of oscillating water column devices. *Journal of Zhejiang University-SCIENCE A (Applied Physics & Engineering)*, 18(5): 329-345. https://doi.org/10.1631/jzus.A1600769

He F, Huang ZH, Law AWK, 2012. Hydrodynamic performance of a rectangular floating breakwater with and without pneumatic chambers: an experimental study. *Ocean Engineering*, 51:16-27. https://doi.org/10.1016/j.oceaneng.2012.05.008

He F, Huang ZH, Law AWK, 2013. An experimental study of a floating breakwater with asymmetric pneumatic chambers for wave energy extraction. *Applied Energy*, 106: 222-231. https://doi.org/10.1016/j.apenergy.2013.01.013

He F, Li MJ, Huang ZH, 2016. An experimental study of pile-supported OWC-type breakwaters: energy extraction and vortex-induced energy loss. *Energies*, 9(7):540. https://doi.org/10.3390/en9070540

He F, Leng J, Zhao XZ, 2017. An experimental investigation into the wave power extraction of a floating box-type breakwater with dual pneumatic chambers. *Applied Ocean Research*, 67:21-30. https://doi.org/10.1016/j.apor.2017.06.009

He F, Zhang HS, Zhao JJ, et al., 2019. Hydrodynamic performance of a pile-supported OWC breakwater: an analytical study. *Applied Ocean Research*, 88:326-340. https://doi.org/10.1016/j.apor.2019.03.022

He F, Liu YB, Pan JP, et al., 2023a. Advanced ocean wave energy harvesting: current progress and future trends. *Journal of Zhejiang University-SCIENCE A (Applied Physics & Engineering)*, 24(2):91-108. https://doi.org/10.1631/jzus.A2200598

He F, Lin Y, Pan JP, et al., 2023b. Experimental investigation of vortex evolution around oscillating water column wave energy converter using particle image velocimetry. *Physics of Fluids*, 35(1):015151. https://doi.org/10.1063/5.0135927

Howe D, Nader JR, Macfarlane G, 2020. Performance analysis of a floating breakwater integrated with multiple oscillating water column wave energy converters in regular and irregular seas. *Applied Ocean Research*, 99:102147. https://doi.org/10.1016/j.apor.2020.102147

Koo W, 2009. Nonlinear time–domain analysis of motion-restrained pneumatic floating breakwater. *Ocean Engineering*, 36(9-10):723-731. https://doi.org/10.1016/j.oceaneng.2009.04.001

Kuo YS, Chung CY, Hsiao SC, et al., 2017. Hydrodynamic characteristics of oscillating water column caisson breakwaters. *Renewable Energy*, 103:439-447. https://doi.org/10.1016/j.renene.2016.11.028

Lee JH, Kwak TY, Jeong YJ, et al., 2023. A study on the lateral load capacity of a novel hybrid monopile via a centrifuge model test. *Energies*, 16(21):7234. https://doi.org/10.3390/en16217234

Li YN, Liu SZ, Xu CL, et al., 2022. Experimental study on the cylindrical oscillating water column device. *Ocean Engineering*, 246:110523. https://doi.org/10.1016/j.oceaneng.2022.110523

Liu ZQ, Fan SL, Wang YZ, et al., 2021. Genetic-algorithm-based layout optimization of an offshore wind farm under real seabed terrain encountering an engineering cost model. *Energy Conversion and Management*, 245: 114610. https://doi.org/10.1016/j.enconman.2021.114610

Liu JB, Song DR, Li QA, et al., 2023. Life cycle cost modelling and economic analysis of wind power: a state of art review. *Energy Conversion and Management*, 277: 116628. https://doi.org/10.1016/j.enconman.2022.116628

Ma HW, Yang J, 2020. A novel hybrid monopile foundation for offshore wind turbines. *Ocean Engineering*, 198:106963. https://doi.org/10.1016/j.oceaneng.2020.106963

Michele S, Renzi E, Perez-Collazo C, et al., 2019. Power extraction in regular and random waves from an OWC in hybrid wind-wave energy systems. *Ocean Engineering*, 191:106519. https://doi.org/10.1016/j.oceaneng.2019.106519

Perez-Collazo C, Greaves D, Iglesias G, 2018. Hydrodynamic response of the WEC sub-system of a novel hybrid wind-wave energy converter. *Energy Conversion and Management*, 171:307-325. https://doi.org/10.1016/j.enconman.2018.05.090

Qu M, Yu DY, Dou ZH, et al., 2021. Design and experimental study of a pile-based breakwater integrated with OWC chamber. *China Ocean Engineering*, 35(3):443-453. https://doi.org/10.1007/s13344-021-0041-0

Ram G, Saad MR, Zainal Abidin N, et al., 2022. Hydrodynamic performance of a hybrid system of a floating oscillating water column and a breakwater. *Ocean Engineering*, 264:112463. https://doi.org/10.1016/j.oceaneng.2022.112463

Schopf W, 2009. Flow Load Controlling Mechanism for Tower of Offshore-Wind Turbine i.e. Monopile, Has Tower Arranged with Flow Resistance-Favorable Surface Structure Such That Sea Current Exerts Smaller Horizontal Forces on Tower. German Patent DE102008008760-A1.

Sheng WN, 2019. Wave energy conversion and hydrodynamics modelling technologies: a review. *Renewable and Sustainable Energy Reviews*, 109:482-498. https://doi.org/10.1016/j.rser.2019.04.030

Shi XL, Liang BC, Du ST, et al., 2022. Wave energy assessment in the china east adjacent seas based on a 25-year wave-current interaction numerical simulation. *Renewable Energy*, 199:1381-1407.

https://doi.org/10.1016/j.renene.2022.09.094

Zhao XL, Li Y, Zou QP, et al., 2022. Long wave absorption by a dual purpose Helmholtz resonance OWC breakwater. *Coastal Engineering*, 178:104203. https://doi.org/10.1016/j.coastaleng.2022.104203

Zheng SM, Zhang YL, Iglesias G, 2019. Coast/breakwater-integrated OWC: a theoretical model. *Marine Structures*, 66:121-135. https://doi.org/10.1016/j.marstruc.2019.04.001

Zheng SM, Antonini A, Zhang YL, et al., 2020a. Hydrodynamic performance of a multi-oscillating water column (OWC) platform. *Applied Ocean Research*, 99:102168. https://doi.org/10.1016/j.apor.2020.102168

Zheng SM, Zhu GX, Simmonds D, et al., 2020b. Wave power extraction from a tubular structure integrated oscillating water column. *Renewable Energy*, 150:342-355. https://doi.org/10.1016/j.renene.2020.01.008

Zhou Y, Ning DZ, Shi W, et al., 2020. Hydrodynamic investigation on an OWC wave energy converter integrated into an offshore wind turbine monopile. *Coastal Engineering*, 162:103731. https://doi.org/10.1016/j.coastaleng.2020.103731

Zhu GX, Graham D, Zheng SM, et al., 2020. Hydrodynamics of onshore oscillating water column devices: a numerical study using smoothed particle hydrodynamics. *Ocean Engineering*, 218:108226. https://doi.org/10.1016/j.oceaneng.2020.108226

Electronic supplementary materials

Figs. S1 and S2